frontiers in Energy Research

ORIGINAL RESEARCH
published: 07 April 2016
doi: 10.3389/fenrg.2016.00012

High Lithium-Ion-Conducting NASICON-Type $Li_{1+x}Al_xGe_yTi_{2-x-y}(PO_4)_3$ Solid Electrolyte

*Shang Xuefu[1,2], Hiroyoshi Nemori[3], Shigehi Mitsuoka[3], Peng Xu[4], Masaki Matsui[1], Yasuo Takeda[1], Osamu Yamamoto[1] and Nobuyuki Imanishi[1]**

[1] Graduate School of Engineering, Mie University, Tsu, Japan, [2] Department of Physics, Faculty of Engineering, Jiangsu University, Zhenjiang, China, [3] Group 4, Component Engineering Development Department, Suzuki Motor Corporation, Hamamatsu, Japan, [4] Department of Physics, Zhejiang University, Hangzhou, China

A water-stable solid electrolyte is a key material without which aqueous lithium–air batteries could not be operated. In this study, we have examined the electrical conductivity and mechanical properties of a water-stable lithium-ion-conducting solid electrolyte, $Li_{1+x}Al_xGe_yTi_{2-x-y}(PO_4)_3$ with the NASICON-type structure, as a function of the Al and Ge content. $Li_{1+x}Al_xGe_yTi_{2-x-y}(PO_4)_3$ was synthesized by the conventional solid-state reaction method. The highest lithium-ion conductivity of 1.0×10^{-3} S cm^{-1} at 25°C and the highest three-point bending strength of 90 N mm^{-2} at room temperature were observed for a pellet of $Li_{1.45}Al_{0.45}Ge_{0.2}Ti_{1.35}(PO_4)_3$ sintered at 900°C.

Keywords: electrical conductivity, lithium–air battery, lithium conductor, NASICON-type, solid electrolyte

OPEN ACCESS

Edited by:
Fuminori Mizuno, Toyota Research Institute of North America, USA

Reviewed by:
Hailei Zhao, University of Science and Technology Beijing, China
Wenping Sun, University of Wollongong, Australia

****Correspondence:***
Nobuyuki Imanishi
imanishi@chem.mie-u.ac.jp

Specialty section:
This article was submitted to Energy Storage, a section of the journal Frontiers in Energy Research

Received: *01 February 2016*
Accepted: *21 March 2016*
Published: *07 April 2016*

Citation:
Xuefu S, Nemori H, Mitsuoka S, Xu P, Matsui M, Takeda Y, Yamamoto O and Imanishi N (2016) High Lithium-Ion-Conducting NASICON-Type $Li_{1+x}Al_xGe_yTi_{2-x-y}(PO_4)_3$ Solid Electrolyte. Front. Energy Res. 4:12. doi: 10.3389/fenrg.2016.00012

INTRODUCTION

In the last half century, many types of lithium-ion-conducting solid electrolytes have been reported, such as Li_3N (Alpen et al., 1977), B_2S_3–Li_2S–LiI glass (Wada et al., 1983), NASICON-type $Li_{1+x}A_xTi_{2-x}(PO_4)_4$ (Aono et al., 1990), perovskite-type $La_{2/3-x}Li_xTiO_3$ (Inaguma et al., 1993), garnet-type $Li_7La_3Zr_2O_{12}$ (Murugan et al., 2007), and thio-LISICON-type $Li_{10}GeP_2S_{12}$ (Kamaya et al., 2011). At present, the highest lithium-ion conductivity of 1.2×10^{-2} S cm^{-1} at room temperature is reported in $Li_{10}GeP_2S_{12}$, which is higher than that of conventional liquid electrolytes, because its lithium-ion transport number is unity. Lithium-ion-conducting solid electrolytes are generally hygroscopic and so are difficult to handle in the open atmosphere, especially the high conductivity sulfide-based solid electrolytes. NASICON-type $Li_{1+x}A_xTi_{2-x}(PO_4)_3$ lithium-conducting solid electrolytes are less sensitive to moisture and can be prepared in the open air, and are also stable in contact with LiCl-saturated aqueous solution (Shimonishi et al., 2011). Aono et al. (1990) has reported the electrical conductivity of the $Li_{1+x}A_xTi_{2-x}(PO_4)_3$ (A = Al, Cr, Ga, Fe, In, La, Sc, and Y) system and found the highest electrical conductivity of 7×10^{-4} S cm^{-1} at 25°C for $Li_{1.3}Al_{0.3}Ti_{1.7}(PO_4)_3$.

Since the report by Aono et al., the NASICON-type lithium-ion-conducting solid electrolytes have been extensively examined. The highest electrical conductivity of 4.62×10^{-3} S cm^{-1} at 27°C was reported for the $Li_{1.5}Al_{0.5}Ge_{1.5}(PO_4)_3$ glass–ceramic by Thokchom and Kumar (2010). However, Fu (1997) studied the $Li_{1-x}Al_xGe_{2-x}(PO_4)_3$ glass–ceramics and found the electrical conductivity of $Li_{1.5}Al_{0.5}Ge_{1.5}(PO_4)_3$ was 4.0×10^{-4} S cm^{-1} at 25°C, and also Xu et al. (2007) found an electrical conductivity of 7.25×10^{-4} S cm^{-1} at room temperature for the $Li_{1.5}Al_{0.5}Ge_{1.5}(PO_4)_3$–0.05 Li_2O glass–ceramic. The preparation of glass–ceramics is somewhat complex, and the effect of aging on the electrical

conductivity is questionable. The $Li_{1+x+y}Al_x(Ge, Ti)_{2-x}Si_yP_{4-y}O_{12}$ glass–ceramics have been commercialized by Ohara, Ltd., Japan. The glass–ceramic is water-permeation free, and the electrical conductivity is 10^{-4} S cm^{-1} at room temperature. Recently, Zhang et al. (2013) reported that the electrical conductivity of $Li_{1.4}Al_{0.4}Ti_{1.6}(PO_4)_3$ was enhanced by a partial substitution of Ge for Ti. The highest electrical conductivity of 1.3×10^{-3} S cm^{-1} at 25°C was observed in $Li_{1.4}Al_{0.4}Ge_{0.2}Ti_{1.4}(PO_4)_3$, where the content of Al was fixed to 0.4, and the $Li_{1.4}Al_{0.4}Ge_xTi_{1.6-x}(PO_4)_3$ powders were prepared by a sol–gel method using expensive Ti and Ge alkoxides. In this study, we have examined the electrical conductivity and mechanical properties of the $Li_{1+x}Al_xGe_yTi_{2-x-y}(PO_4)_3$ system in the range of $x = 0.30$–0.55 and $y = 0.1$–0.3 using less expensive starting materials. Water-stable high lithium-ion-conducting solid electrolytes have potential applications for aqueous lithium–air batteries (Zhang et al., 2010; Bruce et al., 2012) and aqueous lithium batteries with aqueous cathodes (Lu et al., 2011; Zhao et al., 2013). These electrolytes have been used as a protective layer for the lithium metal electrode to avoid direct contact with the aqueous solution, because lithium metal reacts vigorously with water.

MATERIALS AND METHODS

The NASICON-type $Li_{1+x}Al_xGe_yTi_{2-x-y}(PO_4)_3$ lithium-ion-conducting solid electrolytes were prepared by conventional solid-state reaction. Corresponding amounts of chemical reagent grade Li_2CO_3, TiO_2, GeO_2, Al_2O_3, and $NH_4H_2PO_4$ were ball milled with zirconia balls in a zirconia vessel for 2 h at 400 rpm using high energy mechanical milling (HEMM) with a planetary micro mill (Fritsch Pulverisette 7), and the mixed powders were then pressed into pellets at 150 MPa and calcined at 600°C for 4 h. The calcined pellets were reground and again ball milled using HEMM. The obtained powders were isostatically pressed into pellets at 150 MPa and sintered at various temperatures (850–1,000°C) for 7 h. Tape-cast $Li_{1.45}Al_{0.45}Ge_{0.2}Ti_{1.35}(PO_4)_3$ films were prepared using a previously reported method (Zhang et al., 2015). Briefly, fine $Li_{1.45}Al_{0.45}Ge_{0.2}Ti_{1.35}(PO_4)_3$ powders prepared by the solid-state reaction were dispersed in a mixed solution of ethanol and toluene (1:1 v/v) using menhaden fish oil [2 wt% to $Li_{1.45}Al_{0.45}Ge_{0.2}Ti_{1.35}(PO_4)_3$] as a dispersant. The mixed slurry was ball milled for 10 h using HEMM. Polyvinyl alcohol [8 wt% to $Li_{1.45}Al_{0.45}Ge_{0.2}Ti_{1.35}(PO_4)_3$] was then added to the mixed slurry as a plasticizer and ball milled for another 12 h. After tape casting, the green sheets were kept in a sealed box with a small amount of ethanol in a refrigerator to slow the drying process at 5°C for 24 h. Several green sheets were hot pressed at 90°C for 10 min and then sintered at 900°C for 7 h.

The crystal structures of sintered samples were analyzed by X-ray diffraction (XRD) analysis using a Rigaku RINT 2500 diffractometer with Cu-Kα radiation in the 2θ range from 10° to 90° at a scanning step rate of 0.02°s^{-1}. The relative density of the sintered samples was estimated from the ratio of the density calculated from the lattice constants and that calculated from the volume and weight of the sintered body. The electrical conductivity of the sintered pellets (ca. 12 mm diameter and 1 mm thick) with gold sputtered electrodes were measured using an impedance phase analyzer (Solartron 1260) in the frequency range of 0.1 Hz–1 MHz with the bias voltage at 10 mV. Bulk and grain boundary conductivities of the sintered samples were estimated from complex impedance plots using Zview 2. Three-point bending strength of the sintered pellets (ca. 0.24 mm thick and ca. 15 mm wide) was measured at room temperature using a materials tester (Shimadzu EZ-SX 500N).

RESULTS AND DISCUSSION

Figure 1 shows XRD patterns of the $Li_{1.5}Al_{0.5}Ge_{0.2}Ti_{1.3}(PO_4)_3$ samples sintered at various temperatures for 7 h with a silicon internal standard to measure the lattice constant. An impurity phase of $AlPO_4$ was observed for the sample sintered at 850°C. At sintering temperatures as low as 850°C, the reaction was not completed. All diffraction lines of the samples sintered at 900, 950, and 1,000°C could be indexed as the NASICON-type structure (Perez-Estebanez et al., 2014). **Figure 2** shows the relative density of $Li_{1.5}Al_{0.5}Ge_{0.2}Ti_{1.3}(PO_4)_3$ pellets sintered at various temperatures. The sample with the impurity phase that was sintered at 850°C showed a low relative density of 87%. The highest relative density of 95.5% was observed for the sample sintered at 900°C, and the relative density decreased with further increase of the sintering temperature. The decreasing of the relative density may be due to the evaporation of lithium compounds at these higher temperatures. **Figure 3** shows impedance profiles of $Li_{1.5}Al_{0.5}Ge_{0.2}Ti_{1.3}(PO_4)_3$ samples (ca. 1 mm thick) sintered at various temperatures and measured at 25°C. The impedance profiles showed a large semicircle followed by a straight line. The semicircle may be attributed to the grain boundary resistance (Bruce and West, 1983). The intercept of the semicircle on the real axis at high frequency represents the bulk resistance, and the diameter of the semicircle indicates the grain boundary resistance. The semicircle due to the bulk resistance was out of the frequency range for the impedance analyzer used. The samples sintered at 900, 950, and 1,000°C showed almost the same bulk conductivity of ca. 2×10^{-3} S cm^{-1}, while the sample sintered at 850°C showed a low bulk conductivity of ca. 10^{-3} S cm^{-1}. The low bulk conductivity may be due to the non-equilibrium phase of $Li_{1.5}Al_{0.5}Ge_{0.2}Ti_{1.3}(PO_4)_3$ prepared at the lower sintering temperature. The grain boundary resistance was dependent on the sintering temperature, and the sample sintered at 900°C with the highest relative density exhibited the lowest grain boundary resistance.

The electrical conductivity, relative density, and three-point bending strength for the $Li_{1+x}Al_xGe_{0.2}Ti_{1.8-x}(PO_4)_3$ system sintered at 900°C for 7 h were examined as a function of x. **Figure 4** shows the XRD patterns of $Li_{1+x}Al_xGe_{0.2}Ti_{1.8-x}(PO_4)_3$. Almost all the diffraction lines for $Li_{1+x}Al_xGe_{0.2}Ti_{1.8-x}(PO_4)_3$ were indexed with the NASICON-type structure. However, $Li_{1+x}Al_xGe_{0.2}Ti_{1.8-x}(PO_4)_3$ with $x = 0.45$, 0.5, and 0.55 also showed diffraction lines due to $AlPO_4$. The changes in the lattice parameter with x in $Li_{1+x}Al_xGe_{0.2}Ti_{1.8-x}(PO_4)_3$ are shown in **Figure 5**. The a lattice parameter of 0.812 at $x = 0.30$ increased to 0.882 nm at $x = 0.40$, and the c lattice parameter of 2.171 nm decreased to 2.043 nm at $x = 0.4$. Cretin and Fabry (1999) reported that the a parameter decreases and the c parameter increases with increasing x in

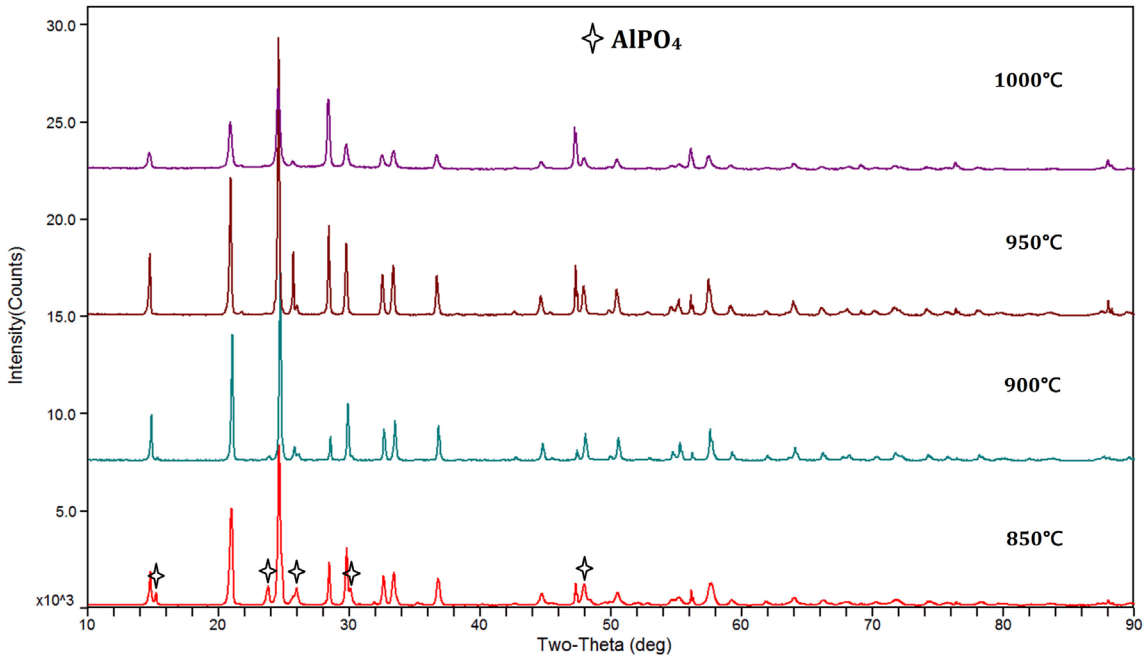

FIGURE 1 | XRD patterns of $Li_{1.5}Al_{0.5}Ge_{0.2}Ti_{1.3}(PO_4)_3$ sintered at various temperatures.

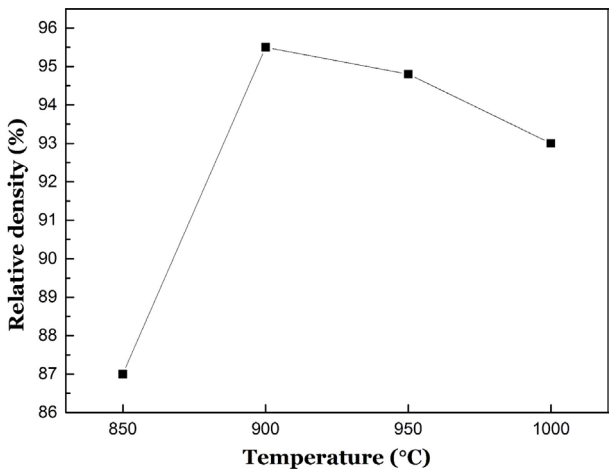

FIGURE 2 | Relative density of $Li_{1.5}Al_{0.5}Ge_{0.2}Ti_{1.3}(PO_4)_3$ sintered at various temperatures.

$Li_{1+x}Al_xTi_{2-x}(PO_4)_3$, while Aono et al. (1990) found both the *a* and *c* parameters decreased with increasing *x*. The decrease of the *c* parameter can be attributed to the substitution of Al^{3+} with a small ionic radius (0.53 nm) for Ti^{4+} with a large ionic radius (0.605 nm) in the octahedral sites. Several factors play a determinant role in the inference of the cation substitution on the structure (Delmas et al., 1981). Additional Li^+ ions are located in the unoccupied Li sites by the substitution of Al^{3+} for Ti^{4+} and Ge^{4+} sites, as observed in $Na_{1+x}Al_xTi_{2-x}(PO_4)_3$ (Maldonado-Manso et al., 2005), to maintain charge neutrality. The additional lithium ions in these sites lead to repulsion along the *a* axis. The reason for the smaller *c* and larger *a* parameters for $Li_{1.55}Al_{0.55}Ge_{0.2}Ti_{1.25}(PO_4)_3$ compared to those for $Li_{1.5}Al_{0.5}Ge_{0.2}Ti_{1.3}(PO_4)_3$ is not clear but may be due to the formation of $AlPO_4$ impurity phases. These results suggest that the solubility limit of Al in $Li_{1+x}Al_xGe_{0.2}Ti_{1.8-x}(PO_4)_3$ is $x = 0.4$, as observed by Aono et al. (1990) for $Li_{1+x}Al_xTi_{2-x}(PO_4)_3$. **Figure 6** shows impedance profiles for $Li_{1+x}Al_xGe_{0.2}Ti_{1.8-x}(PO_4)_3$ measured at 25°C as a function of *x*. The lowest grain boundary resistance was observed for $Li_{1.45}Al_{0.45}Ge_{0.2}Ti_{1.35}(PO_4)_3$. The equivalent circuit in **Figure 6** assumes a general model comprising grains and uniform grain boundaries that are parallel or perpendicular to the current flow. This results in the one with two parallel resistance–capacitance elements, one for the perpendicular grain boundary (R_{p1} and CPE_1) and one from the parallel grain boundary (R_{p2} and CPE_2) connected in parallel. In microcrystalline ceramics, where the effective grain boundary width is negligible compared to the grain size, the contribution of the parallel grain boundary can be neglected. However, parallel grain boundary contribution must be taken into account if the parallel grain boundary conductivity becomes significantly larger than that of the grain and/or if the effective grain boundary width is no longer negligible with respect to the grain size (Bouchet et al., 2003). The change in the grain boundary resistance with *x* could be explained by the change of the relative density as shown in **Figure 7**. $Li_{1.55}Al_{0.55}Ge_{0.2}Ti_{1.25}(PO_4)_3$ with the $AlPO_4$ impurity phase had similar impedance profiles to those of $Li_{1.50}Al_{0.5}Ge_{0.2}Ti_{1.3}(PO_4)_3$ with the $AlPO_4$ impurity phase sintered at 850°C, which revealed a high grain boundary resistance and low bulk conductivity. **Figure 7** shows the electrical conductivities of total, grain bulk, grain boundary, and the relative density of $Li_{1+x}Al_xGe_{0.2}Ti_{1.8-x}(PO_4)_3$ measured at 25°C that are plotted as a function of *x*. The highest total conductivity of

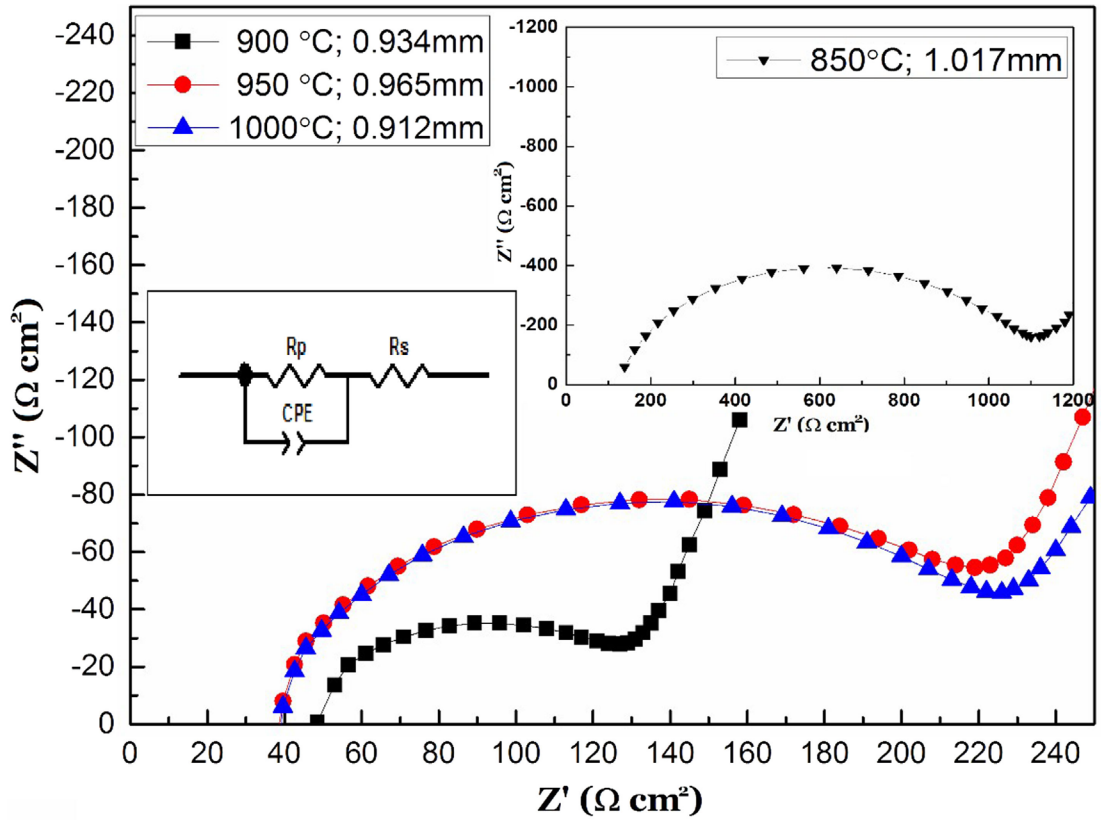

FIGURE 3 | **Impedance profiles of Au/$Li_{1.5}Al_{0.5}Ge_{0.2}Ti_{1.3}(PO_4)_3$/Au as a function of the sintering temperature**.

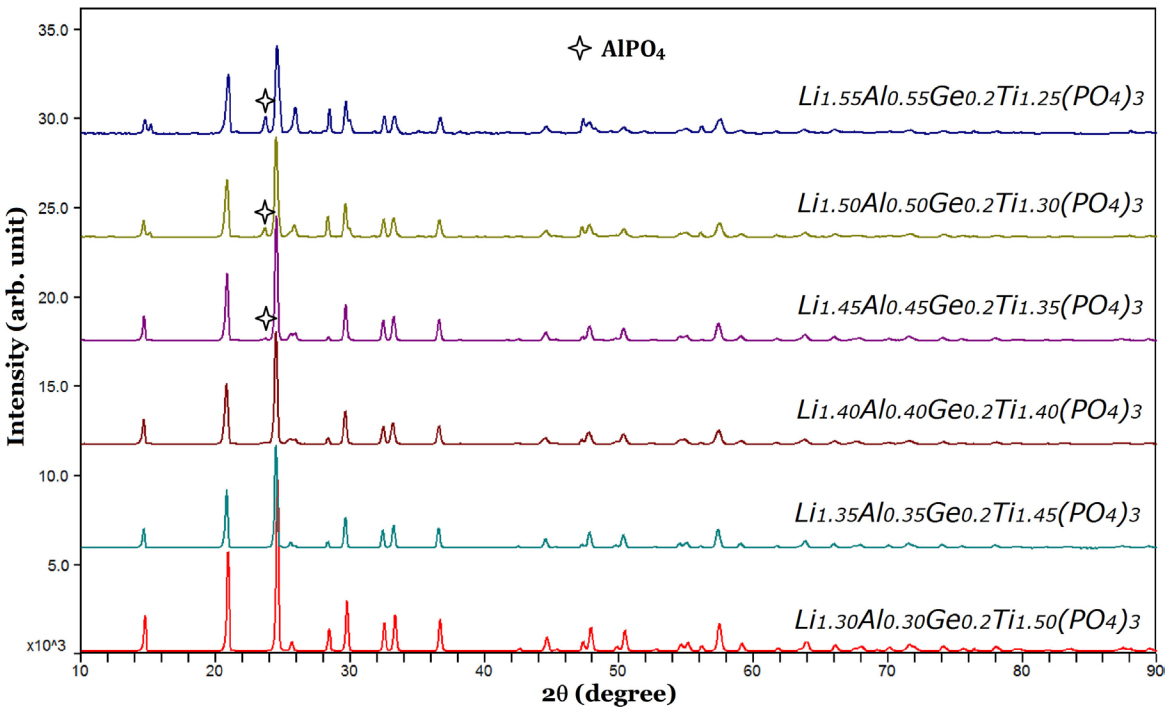

FIGURE 4 | **XRD patterns of $Li_{1+x}Al_xGe_{0.2}Ti_{1.8-x}(PO_4)_3$ sintered at 900°C as a function of *x***.

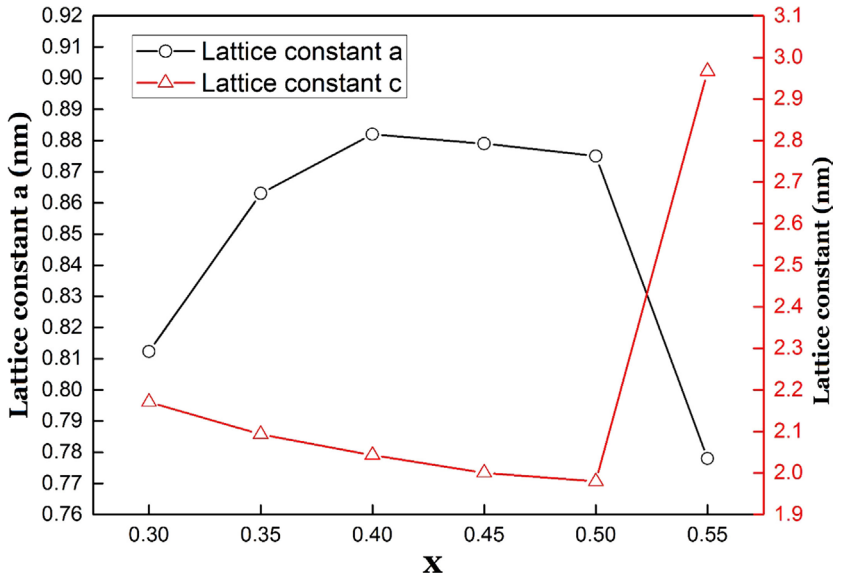

FIGURE 5 | Lattice parameter for $Li_{1+x}Al_xGe_{0.2}Ti_{1.8-x}(PO_4)_3$ sintered at 900°C as a function of *x*.

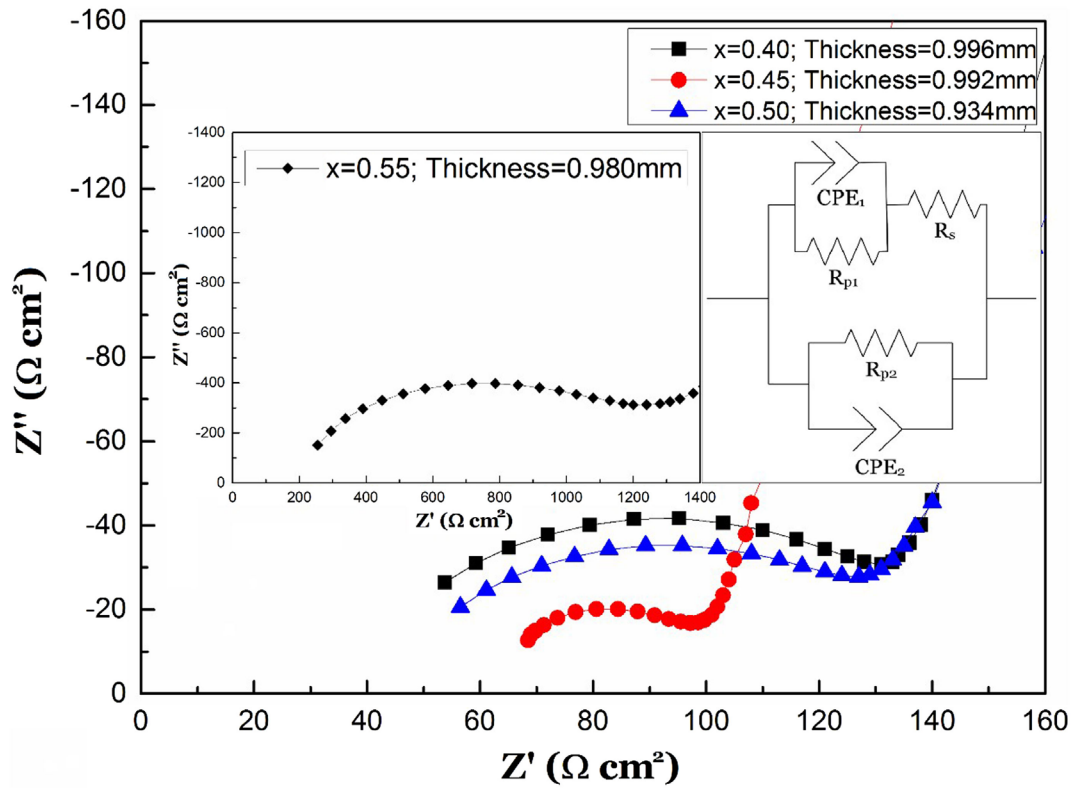

FIGURE 6 | Impedance profiles for $Li_{1+x}Al_xGe_{0.2}Ti_{1.8-x}(PO_4)_3$ measured at 25°C as a function of *x*.

1.0×10^{-3} S cm^{-1} and the highest relative density of 95.8% were observed for $Li_{1.45}Al_{0.45}Ge_{0.2}Ti_{1.35}(PO_4)_3$ at $x = 0.45$. The grain bulk conductivities at $x = 0.40$ and 0.50 are higher than that at $x = 0.45$. The reason for this tendency is not yet clarified. Aluminum composition in the grain bulk may slightly deviate from the nominal one by its accumulation at the grain boundary region.

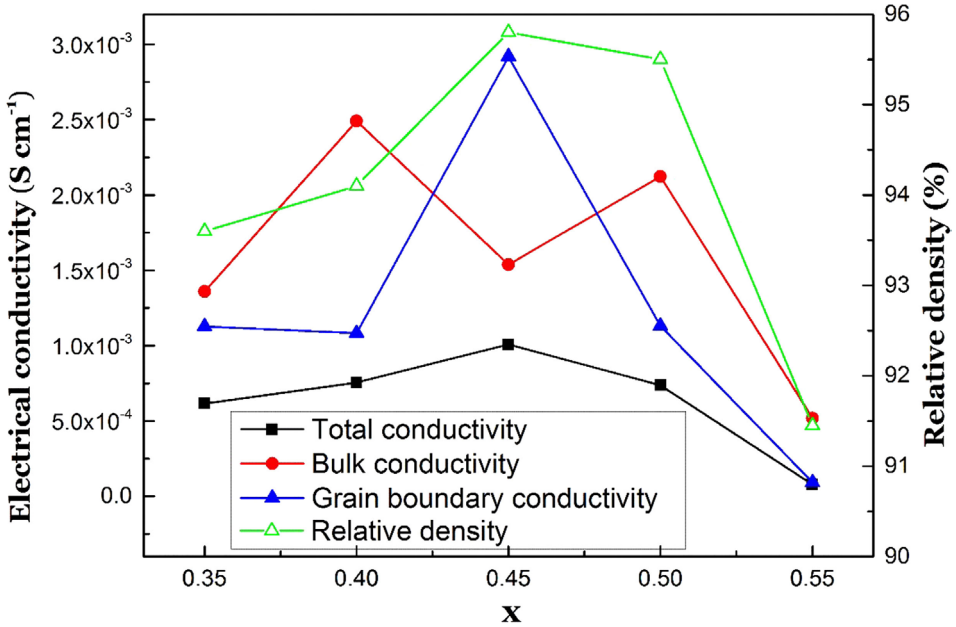

FIGURE 7 | Total, bulk, and grain boundary electrical conductivity at 25°C, and relative density of $Li_{1+x}Al_xGe_{0.2}Ti_{1.8-x}(PO_4)_3$ as a function of *x*.

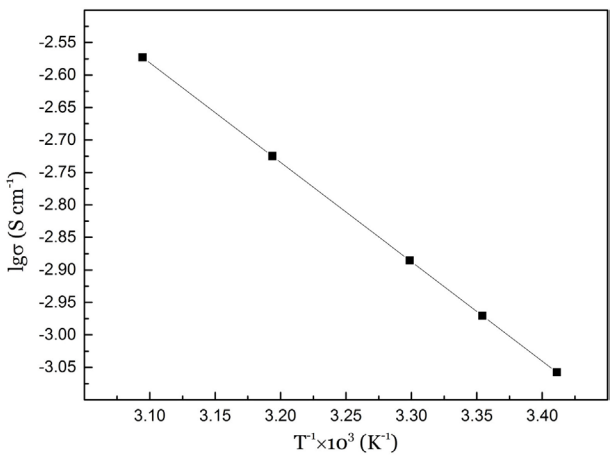

FIGURE 8 | Temperature dependence of the electrical conductivity of $Li_{1.45}Al_{0.45}Ge_{0.2}Ti_{1.35}(PO_4)_3$.

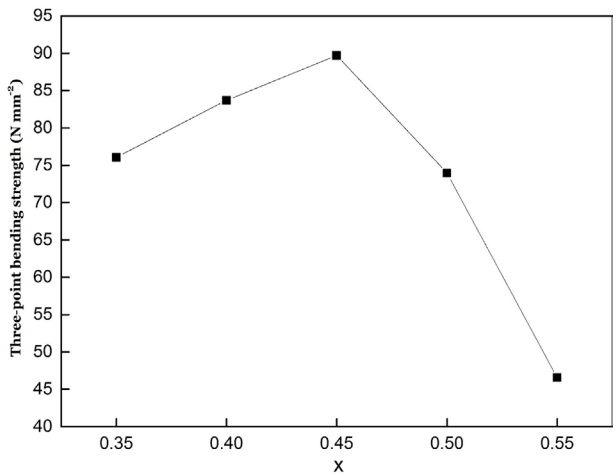

FIGURE 9 | Three-point bending strength of $Li_{1+x}Al_xGe_{0.2}Ti_{1.8-x}(PO_4)_3$ as a function of *x*.

As another thought, the estimation of the bulk conductivity could be influenced by a parallel grain boundary conduction path as illustrated in the equivalent circuit in **Figure 6**, although the grain boundary conductivities of $Li_{1+x}Al_xGe_{0.2}Ti_{1.8-x}(PO_4)_3$ at $x = 0.40$ and 0.50 were lower than that for $Li_{1.45}Al_{0.45}Ge_{0.2}Ti_{1.35}(PO_4)_3$. As a rough tendency, it is possible to state that conductivity becomes maximum around $x = 0.45$, and as leaving from the composition, the bulk and the grain boundary conductivity decreases. **Figure 8** shows the temperature dependence of the total electrical conductivity for $Li_{1.45}Al_{0.45}Ge_{0.2}Ti_{1.35}(PO_4)_3$. The activation energy for the electrical conduction was calculated to be 31 kJ mole^{-1}, which is comparable to that for $Li_{1.4}Al_{0.4}Ge_{0.2}Ti_{1.4}(PO_4)_3$, as reported previously (Zhang et al., 2013). **Figure 9** shows the dependence of the three-point bending strength on the Al content for $Li_{1+x}Al_xGe_{0.2}Ti_{1.8-x}(PO_4)_3$ sintered at 900°C for 7 h. The maximum bending strength of 90 N mm^{-2} was observed for $Li_{1.45}Al_{0.45}Ge_{0.2}Ti_{1.35}(PO_4)_3$ with a relative density of 95.8%. The bending strength is higher than that of 65 N mm^{-2} for

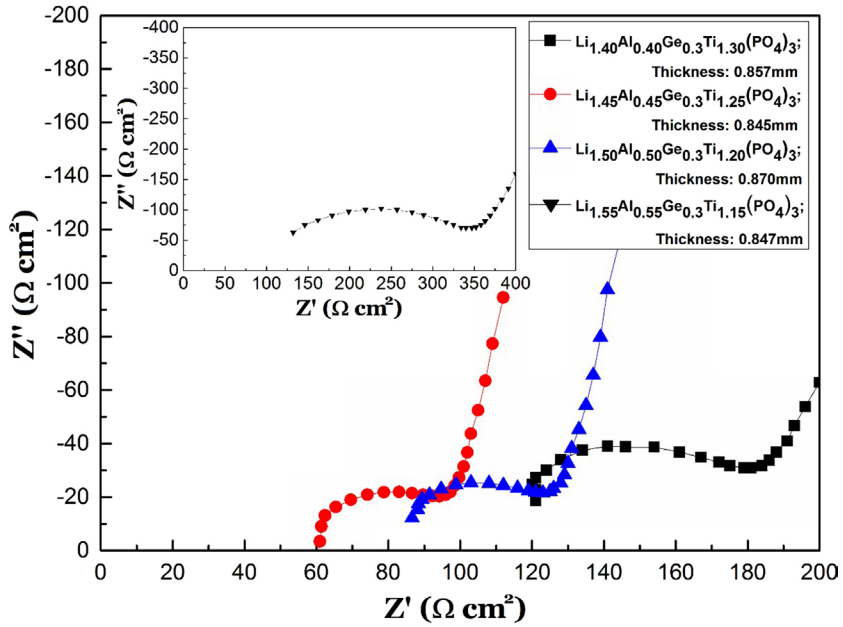

FIGURE 10 | **Impedance profiles measured at 25°C of $Li_{1+x}Al_xGe_{0.3}Ti_{1.7-x}(PO_4)_3$ as a function of *x*.**

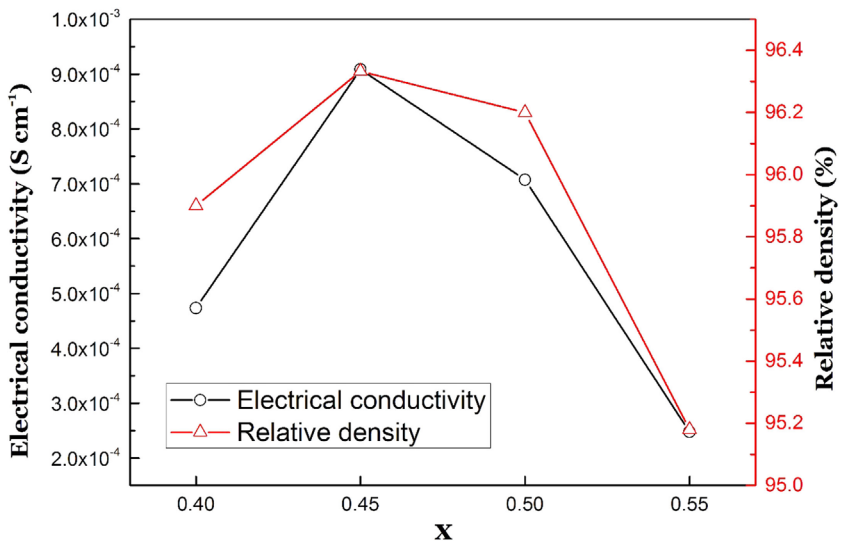

FIGURE 11 | **Total electrical conductivity at 25°C and relative density of $Li_{1+x}Al_xGe_{0.3}Ti_{1.8-x}(PO_4)_3$ as a function of *x*.**

$Li_{1.4}Al_{0.4}Ge_{0.2}Ti_{1.4}(PO_4)_3$ prepared by tape casting using powder prepared by the sol–gel method (Zhang et al., 2015) and lower than that of 140 N mm^{-2} for a polished Ohara plate of $Li_{1+x+y}Al_x(Ti,Ge)Si_yP_{3-y}O_{12}$ glass–ceramics, the conductivity of which is as low as 1×10^{-4} S cm^{-1} at room temperature. The high bending strength of $Li_{1.45}Al_{0.45}Ge_{0.2}Ti_{1.35}(PO_4)_3$ prepared by the conventional solid-state reaction is quite attractive for applications, such as the water-stable protective layer in aqueous lithium batteries.

Zhang et al. (2013) examined the electrical conductivity dependence on the Ge content in $Li_{1.4}Al_{0.4}Ge_xTi_{1.6-x}(PO_4)_3$, and the highest conductivity was observed for $Li_{1.4}Al_{0.4}Ge_{0.2}Ti_{1.4}(PO_4)_3$ prepared by the sol–gel method. We also examined the effect of the Ge content in $Li_{1+x}Al_xGe_yTi_{2-x-y}(PO_4)_3$. **Figure 10** shows impedance profiles measured at 25°C of $Li_{1+x}Al_xGe_{0.3}Ti_{1.7-x}(PO_4)_3$ as a function of *x*. The highest bulk conductivity of 1.39×10^{-3} S cm^{-1} and total conductivity of 8.95×10^{-4} S cm^{-2} were observed for

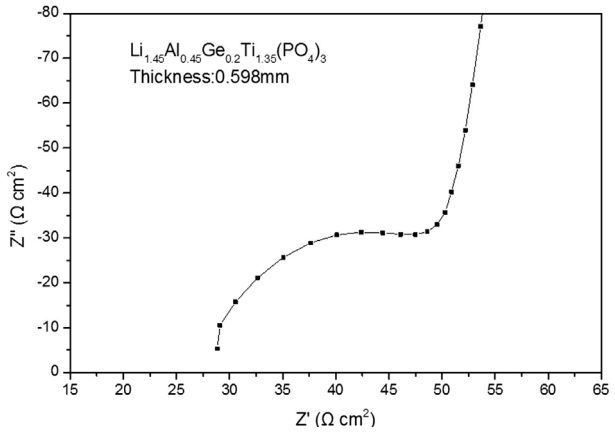

FIGURE 12 | Impedance profile of the tape cast $Li_{1.45}Al_{0.45}Ge_{0.2}Ti_{1.35}(PO_4)_3$ film measured at 25°C.

$Li_{1.45}Al_{0.45}Ge_{0.3}Ti_{1.25}(PO_4)_3$. The total conductivity and relative density of $Li_{1+x}Al_xGe_{0.3}Ti_{1.7-x}(PO_4)_3$ are shown as a function of x in **Figure 11**. The bulk conductivities of $Li_{1.5}Al_{0.5}Ge_{0.3}Ti_{1.2}(PO_4)_3$ and $Li_{1.4}Al_{0.4}Ge_{0.3}Ti_{1.3}(PO_4)_3$ are considerably lower than those of $Li_{1.5}Al_{0.5}Ge_{0.2}Ti_{1.3}(PO_4)_3$ and $Li_{1.4}Al_{0.4}Ge_{0.2}Ti_{1.4}(PO_4)_3$, respectively. The highest relative density of 96.3% was observed for $Li_{1.45}Al_{0.45}Ge_{0.3}Ti_{1.25}(PO_4)_3$. The $Li_{1.5}Al_{0.5}Ge_{0.1}Ti_{1.4}(PO_4)_3$ sample with a low Ge content had a low total conductivity of 2.7×10^{-4} S cm^{-1} and a low grain boundary conductivity of 3.3×10^{-4} S cm^{-1} at 25°C.

The tape casting method is suitable to prepare solid electrolytes for the large size batteries in electric vehicles and stationary electricity storage systems. Takahashi et al. (2012) reported the electrical conductivity for a tape-cast $Li_{1.4}Al_{0.4}Ti_{1.6}(PO_4)_3$–3 wt% TiO_2 film as 7.6×10^{-4} S cm^{-1} at 25°C. Zhang et al. (2015) also reported an electrical conductivity of 1.22×10^{-3} S cm^{-1} at 25°C for a tape-cast film of $Li_{1.4}Al_{0.4}Ge_{0.2}Ti_{1.4}(PO_4)_3$. The powders for these tape casting films were prepared by the sol–gel method using expensive Ti and Ge alkoxides. Here, we prepared $Li_{1.45}Al_{0.45}Ge_{0.2}Ti_{1.35}(PO_4)_3$ films by the tape casting method using powders prepared by the conventional solid-state reaction using TiO_2 and GeO_2. The impedance profile of the film measured at 25°C is shown in **Figure 12**. Zhang et al. (2015) reported an aging effect on the electrical conductivity of a tape-cast film stored in an air atmosphere. Therefore, the impedance was measured for a film stored for 1 week in an Ar glove box. The total and bulk conductivities at 25°C were estimated to be 1.01×10^{-3} and 2.21×10^{-3} S cm^{-1}, respectively, which are comparable to those of a sintered plate prepared from a pressed green body.

CONCLUSION

The NASICON-type water-stable lithium-ion-conducting solid electrolyte of $Li_{1+x}Al_xGe_yTi_{2-x-y}(PO_4)_3$ was prepared using conventional solid-state reaction at 900°C for 7 h. The highest lithium-ion conductivity of 10^{-3} S cm^{-1} at 25°C was found for the $Li_{1+x}Al_xGe_yTi_{2-x-y}(PO_4)_3$ composition with $x = 0.45$ and $y = 0.2$. The relative density of the sintered pellets was as high as 95.8%, and the three-point bending strength was 90 N mm^{-2}. Tape cast films of $Li_{1.45}Al_{0.45}Ge_{0.2}Ti_{1.35}(PO_4)_3$ were prepared using powder prepared by solid-state reaction. The total and bulk electrical conductivities of the film were comparable with those of a sintered plate prepared from a pressed green body. This water-stable high lithium-ion-conducting solid electrolyte has potential application as the protective layer of lithium metal electrodes in aqueous lithium–air batteries and lithium batteries with aqueous liquid cathodes.

AUTHOR CONTRIBUTIONS

SX, HN, and PX did preparation of NASICON-type oxide, characterization, and conductivity measurements. SX also did the tape casting of the ceramics. SM, MM, YT, and OY supported and gave an advice on each experimental work. NI managed the research direction and provided necessary instructions and opportunities for discussions among all authors.

REFERENCES

Aono, H., Sugimoto, E., Sadaoka, Y., Imanaka, S., and Adachi, G. (1990). Ionic conductivity of solid electrolyte based on lithium titanium phosphate. *J. Electrochem. Soc.* 137, 1023–1027. doi:10.1149/1.2086597

Alpen, U. V., Rubenau, A., and Talt, G. H. (1977). Ionic conducting in Li_3N single crystal. *Appl. Phys. Lett.* 30, 621–623. doi:10.1063/1.89283

Bouchet, R., Knauth, P., and Laugler, J. M. (2003). Theoretical analysis of IS of polycrystalline materials with blocking or conducting grain boundary: from microcrystals to nanocrystals. *J. Electrochem. Soc.* 150, E348–E354. doi:10.149/1.1580151

Bruce, P. G., Feunberger, S. A., Hardwick, L. J., and Tarascon, J. M. (2012). Li-O_2 and Li-S batteries with high energy storage. *Nat. Mater.* 11, 19–29. doi:10.1038/nmat3191

Bruce, P. G., and West, A. R. (1983). The A-C conductivity of polycrystalline LISICON $Li_{2+2x}Zn_{1+x}GeO_4$ and a model for the intergranular construction resistance. *J. Electrochem. Soc.* 130, 662–669. doi:10.1149/1.2119778

Cretin, M., and Fabry, P. (1999). Comparative study of lithium ion conductors in the system $Li_{1+x}Al_xA_{2-x}^{IV}(PO_4)_3$ with A^{IV}=Ti or Ge and $0 \leq x \leq 0.7$ for use as Li^+ sensitive membranes. *J. Eur. Ceram. Soc.* 19, 2931–2940. doi:10.1016/s0955-2219(99)00055-2

Delmas, C., Viala, J. C., Olazcuage, R., Le Flem, G., Hagnemuller, P., and Chrkaoui, F. (1981). Conductivite ionique dnas les systmes $Na_{1+x}Zr_{2+x}L_x(PO_4)_3$(L=Cr, Yb). *Mater. Res. Bull.* 16, 83–90. doi:10.1016/0025-5408(81)90182-3

Fu, J. (1997). Fast Li^+ ion conducting glass-ceramics in the system Li_2O-Al_2O_3-GeO_2-P_2O_5. *Solid State Ionics.* 104, 191–194. doi:10.1016/s0167-2738(99)00434-7

Inaguma, N., Chen, L., Itoh, M., Nakamura, T., Uchida, T., Ikuta, H., et al. (1993). High ionic conductivity in lithium lanthanum titanate. *Solid State Commun.* 86, 689–693. doi:10.1016/0038-1098(93)90841-A

Kamaya, N., Honma, K., Yamakawa, Y., Nakamura, T., Hirayama, M., Kanno, R., et al. (2011). A lithium super ionic conductor. *Nat. Mater.* 10, 682–686. doi:10.1038/nmat.3066

Lu, Y., Goodenough, J. R., and Kim, Y. (2011). Aqueous cathode for next-generation alkali-ion batteries. *J. Am. Chem. Soc.* 133, 5756–5759. doi:10.1021/ja.201118f

Maldonado-Manso, P., Aranda, M. A. G., Bruque, J. S., and Losilla, E. R. (2005). Nominal vs. actual stoichiometries in Al-doped NASICONs; a study of the $Na_{1.4}Al_{0.4}M_{1.6}(PO_4)_3$ (M=Ge, Sn, Ti, Hf, Zr) family. *Solid State Ionics* 176, 1613–1625. doi:10.1016/jss.2005.04.009

Murugan, R., Thangadurai, V., and Weppner, W. (2007). Fast lithium ion conduction in garnet-type $Li_7La_3Zr_2O_{12}$. *Angew. Chem. Int. Ed.* 46, 7778–7781. doi:10.1002/anie.200701144

Perez-Estebanez, M., Lasai-Marin, J., Tobbens, D. M., Rivera-Calzada, A., and Leon, C. (2014). A systematic study on NASICON-type $Li_{1+x}M_xTi_{2-x}(PO_4)_3$ (M=Cr, Al, Fe,) by neutron diffraction and impedance spectroscopy. *Solid State Ionics* 266, 1–8. doi:10.1016/j.ssi.2014.07.018

Shimonishi, Y., Zhang, T., Imanishi, N., Im, D., Lee, D. I., Hirano, A., et al. (2011). A study on lithium/air second batteries – stability of the NASICON-type lithium ion conducting solid electrolyte in alkaline aqueous solution. *J. Power Sources* 196, 5128–4133. doi:10.1016/jpowersouce.2011.02.023

Takahashi, K., Johnson, P., Imanishi, N., Sammes, N., Takeda, Y., and Yamamoto, O. (2012). A water-stable high lithium ion conducting $Li_{1.4}Ti_{1.6}Al_{0.4}(PO4)_3$-epoxy resin hybrid sheet. *J. Electrochem. Soc.* 159, A1065–A1069. doi:10.1149/2.072207jes

Thokchom, J. S., and Kumar, B. (2010). The effects of crystallization parameters on the ionic conductivity of a lithium aluminum germanium phosphate glass ceramics. *J. Power Sources* 195, 2870–2879. doi:10.1018/j.powersouces.2009.11.037

Wada, H., Menetrierm, A., Lavasseurs, A., and Hagenmuller, P. (1983). Preparation and ionic conductivity of new B_2S_3-Li_2S-LiI glass. *Mater. Res. Bull.* 18, 189–192. doi:10.1018/0025-5408(83)90080-6

Xu, X., Wen, Z., Wu, X., Yang, X., and Gu, Z. (2007). Lithium ion-conducting glass-ceramics of $Li_{1.5}Al_{0.5}Ge_{1.5}(PO_4)_3$-$xLi_2O$ (x=0.0-0.20) with good electrical and electrochemical properties. *J. Am. Ceram. Soc.* 90, 2802–2806. doi:10.1111/j.1511-2916.207.01827.x

Zhang, P., Matsui, M., Hirano, A., Takeda, Y., Yamamoto, O., and Imanishi, N. (2013). Water-stable lithium ion conducting solid electrolyte of the $Li_{1.4}Al_{0.4}Ti_{1.6-x}Ge_x(PO_4)_3$ system (A=x=0-1.0) with NASICON-type structure. *Solid State Ionics* 253, 175–180. doi:10.1016/j.ssi.2013.09.022

Zhang, P., Wang, H., Lee, Y.-G., Matsui, M., Takeda, Y., Yamamoto, O., et al. (2015). Tape-cast water-stable NASICON-type high lithium ion conducting solid electrolyte films for aqueous lithium-air batteries. *J. Electrochem. Soc.* 162, A1265–A1271. doi:10.1149/2.0711507jes

Zhang, T., Imanishi, N., Shimonishi, Y., Hirano, A., Takeda, Y., Yamamoto, O., et al. (2010). A novel high energy rechargeable lithium/air battery. *Chem. Commun.* 46, 1661–1663. doi:10.1039/b926012f

Zhao, Y., Wang, L., and Byon, H. R. (2013). High-performance rechargeable lithium-iodine batteries using triiodide/iodide redox couples in an aqueous cathode. *Nat. Commun.* 4, 1896. doi:10.1038/ncomms2907

Conflict of Interest Statement: The authors declare that the research was conducted in the absence of any commercial or financial relationships that could be construed as a potential conflict of interest.

Copyright © 2016 Xuefu, Nemori, Mitsuoka, Xu, Matsui, Takeda, Yamamoto and Imanishi. This is an open-access article distributed under the terms of the Creative Commons Attribution License (CC BY). The use, distribution or reproduction in other forums is permitted, provided the original author(s) or licensor are credited and that the original publication in this journal is cited, in accordance with accepted academic practice. No use, distribution or reproduction is permitted which does not comply with these terms.